Bull Earthquake Eng (2016) 14:1195–1217
DOI 10.1007/s10518-016-9867-x

ORIGINAL RESEARCH PAPER

Estimating ground motion incoherence through finite source simulation: a case study of the 1980 El-Asnam Earthquake

K. AfifChaouch[1] · B. Tiliouine[1] · M. Hammoutene[1] · R. Sigbjörnsson[2] · R. Rupakhety[2]

Received: 28 July 2015 / Accepted: 8 January 2016 / Published online: 25 January 2016

Abstract Spatial variability of ground motions has significant influence on dynamic response of extended structures such as bridges and tunnels. In this study, the widely used finite-source ground motion simulation approach, the so-called Empirical Green's Function (EGF) method, is extended to synthesize seismic motions across an array of stations located at bedrock in the epicentral region of the 1980 El-Asnam region (North-West Algeria). The target event being simulated is the October 10 1980 $M_s = 7.2$ Earthquake, and the EGF is obtained from the ground motion recorded at Sogedia Factory station during the 8 November 1980 $M_L = 5.6$ aftershock. Coherency functions are then estimated from the simulated ground accelerations. A parametric study investigating the influence of shear wave velocity, earthquake magnitude, and epicentral distance is conducted by simulating ground acceleration for different scenarios using the Hybrid Green's Function method. The main finding of the study is that finite source effects can cause significant loss in coherency at bedrock in the near-field. In the far-field, the source effect alone does not seem to produce incoherent motion, which implies that scattering and local site effects could be dominating there. Furthermore, coherency functions are found to be more sensitive to inter-station separation in the near-field than in the far-field. Increasing shear wave velocity seems to increase coherency functions, and larger earthquakes seem to produce more incoherent motion than smaller ones. The simulation method presented here produces incoherent motion mainly due to the finite source effect, while path effects are partially accounted for through the EGF, and local site effects are not considered. In this sense, the estimated coherency functions represent that of plane waves. A parametric model of plane wave coherency is calibrated and presented based on the simulation results. The results indicate that the parametric model can be used as a first approximation, and at least an upper bound of lagged coherency in the near-field region of the El-Asnam Earthquake

✉ R. Rupakhety
rajesh@hi.is

[1] LGSDS, Seismic Engineering and Structural Dynamics Laboratory, National Polytechnic School, Algiers, Algeria

[2] Earthquake Engineering Research Centre (EERC), University of Iceland, Selfoss, Iceland

scenario. This model could be useful in random vibration analysis or generation of spatially variable ground motion for time history analysis of lifeline structures in the study area.

Keywords Ground motion simulation · Green's function · Finite source · Lifeline · Coherency · El-Asnam Earthquake

1 Introduction

Lifelines systems such as gas mains, oil pipelines, bridges, dams etc., which are supported on ground over large horizontal distances experience differential seismic movement of their supports during earthquakes. This differential motion of the supports results in displacement and stress distribution in the structural elements that are different than what is caused by uniform motion of all the supports. In many cases, the outcome is additional strain (or stress) on the elements, which can, in the event of strong shaking, result in damage to the elements of the such structures (e.g., Zerva 1994; Harichandran and Wang 1990; Lupoi et al. 2005; Walling and Abrahamson 2007; Nazmy and Abdel-Ghaffar 1992). Spatial variation of ground motion results from different physical processes related to the seismic source, the wave propagation path, and local site conditions. Attenuation effects result in reduction of ground motion amplitudes with distance from the source. At a local spatial scale, for example within a few hundred meters, the attenuation effect is not critical, and spatial variation is due to physical processes such as (1) wave passage effects, which refer to the difference in arrival times of seismic waves at different locations; (2) incoherence effects, which refer to the differences in amplitudes and phases due to multiple reflections and refractions of seismic waves in inhomogeneous medium, as well as the complex superposition of waves radiated from different parts of the source; and (3) local site effects, which refer to the change in amplitude and frequency content of ground motion due to local variation of soil conditions.

When the soil medium is locally uniform, variability in amplitude and frequency content is less significant than variations in phase caused by wave passage and incoherence effects. In such situations, ground motion variability is locally modelled as realizations of random processes with spatially uniform amplitude and frequency content (Der Kiureghian 1996). Engineering models of such processes are often calibrated from strong-motion array data from past earthquakes. This includes estimation of apparent wave propagation velocity, the coherence function, and the site-dependent power spectral density function of seismic waves. Several models of coherency and correlation functions, both theoretical and empirical, are reported in the literature (see, for example, Der Kiureghian 1996; Harichandran and Vanmarcke 1986; Abrahamson et al. 1991b; Luco and Wong 1986). Such models are needed in simulating time series of spatially variable ground motion which are required in seismic response analysis of horizontally extended structures. It is well known that coherency functions are characteristic of a local site, source, and wave propagation path, and therefore models calibrated from data collected in one region may not be suitable for use in other areas (Somerville et al. 1988, 1991; Oliveira et al. 1991; Abrahamson et al. 1991a; Santa-Cruz et al. 2000; Ding et al. 2004). Despite this, due to lack of local data, coherency models calibrated for one region are often used to simulate ground motion in other regions, sometimes with different tectonic and geological settings.

Although strong motion networks are expanding in many countries, dense arrays, which are required to record local variability, are still rare. An alternative method to simulate spatially variable ground motion when recorded data is lacking could be numerical simulation of ground motion. In this context, stochastic simulation methods (Hao et al. 1989; Bi and Hao 2012; Oliveira et al. 1991; Shinouzuka et al. 1987) which require pre-specified coherency functions are not applicable and one needs to resort to simulation based on the physics of seismic source and wave propagation. The choice of an appropriate simulation method depends on the availability of data on the wave propagation path and seismic source. The simulation method should be capable of incorporating the physical effects (e.g. the finite source effect) that lead to spatial variability at a local scale that conform to the current empirical and theoretical understanding of spatial and spectral nature of coherency functions (Schneider et al. 1992; Ding et al. 2004; Ding and Song 2010; Menke et al. 1990; Horike and Takeuchi 1996).

The two widely-used ground motion simulation approaches rely on point-source and finite-source modelling. The point-source method (Boore 1983, 2003; Boore and Atkinson 1987; Hao and Gaull 2004) lacks the ability to model incoherence effects due to seismic waves radiated from different parts of a finite source. Such effects can be at least partially incorporated in finite-source ground motion simulation methods. Such methods rely on modelling an extended earthquake source and the wave propagation medium. Numerical simulations of ground motion incorporating the effects of a three-dimensional seismic source, wave propagation in complex media, as well as the influence of the local site—such as, topographic effects and basin response—have gained popularity in the recent years (see, for example, Bielak et al. 2010; and Smerzini and Villani 2012). Such simulations are often deterministic numerical methods based on Finite Elements (Bielak et al. 2005), Finite Differences (Graves 1996; Pitarka 1999) or Spectral Elements (Faccioli et al. 1997; Komatitsch and Vilotte 1998: Mazzieri et al. 2013). Such extensive simulation methods are very attractive due to their ability to model complex source, path, and site effects in generation and propagation of three-dimensional seismic wave field. These methods are, however, computationally expensive and require knowing the source as well as geological and geotechnical properties of the area in great detail. The results of such simulations are accurate, like any other simulation, to the same degree that the input data are accurate. In other words, detailed information on the fault geometry and slip distribution, as well as the geological structure of the site is required. While such information can be compiled for recent large earthquakes, it is not easily predicted for future earthquakes. In this sense, although such methods have been very successful in reproducing ground-motion records from well-studied past earthquakes, their reliability in predicting ground motion due to a future earthquake depends on the level of confidence with which various source, path, and site parameters are predicted. Through detailed geological and geotechnical studies, uncertainties in the path and site parameters can potentially be reduced, but, inherent uncertainties in source parameters, such as slip distribution, are still significant; it is not yet possible to predict the source model of a future earthquake based on past experience. Most importantly, these physics-based, numerical methods can simulate only low-frequency (to about 2.5 Hz; see for example, Smerzini and Villani 2012) motion. For engineering applications, and especially for incoherence effects, larger frequency components ($\sim$2–9 Hz) are more relevant. Hybrid methods of simulation where low-frequency motion obtained from physics-based models are combined with high-frequency motion obtained from stochastic models have been developed in recent years (see, for example, Mai et al. 2010; Graves and Pitarka 2010; Aagaard et al. 2010). Due to the computational cost and

lack of detailed information about the source, path, and site, these models have limited use in routine work.

An alternative to modelling the wave propagation effect is provided by the use of the so-called Empirical Green's Functions (EGF). These functions are calibrated from ground motion time series recorded during small events and, in this sense, incorporate, at least partially, the effect of wave the propagation path. The small event must correspond to the same seismogenic source as the target event being simulated. Hartzell (1978) first utilized observed records from small events (e.g., aftershocks and foreshocks) as Green's functions to simulate ground motion time series corresponding to a mainshock. Since then, his original idea has been applied, developed, and improved by numerous researchers (e.g., Kanamori 1979; Hadley and Helmberger 1980; Mikumo et al. 1981; Irikura and Muramatu 1982; Kamae and Irikura 1998; Irikura 1983, 1986; Irikura et al. 1997). Sometimes, EGF in the form of recorded time series from small earthquakes are not available. In these cases, the EGF method as originally developed is not applicable. To overcome this problem, hybrid methods for broad-band ground motion simulation have been developed combining deterministic and stochastic approaches. One such method is the Hybrid Green's Function (HGF) technique proposed by Kamae et al. (1998a). In this semi-empirical method, ground motion time histories corresponding to small earthquake events are calculated theoretically using the stochastic point-source model (Boore 1983; Hao and Gaull 2004), which are then used as EGF to simulate the ground motion corresponding to large earthquakes. This approach has been used in simulating strong motion time series in regions where recorded data is not available (Suzuki and Asano 2000; Joshi and Midorikawa 2004; Joshi and Mohan 2008; Liang et al. 2006, 2008).

In the following sections, we provide a brief review of the EGF and the HGF method for ground motion simulation, and explain their application in simulating spatially variable ground motion. Basic definitions and spectral methods used in evaluating ground motion coherency are also reviewed. A case study of the 1980 El-Esnam Earthquake is presented, with simulated coherency functions at bedrock in the near-field. This is followed by a parametric study investigating the effects of shear wave velocity, earthquake magnitude, and epicentral distance on simulated coherency functions. The results are compared with published literature, and they are interpreted in light of the physics of ground motion generation incorporated in the simulation methods. Based on the simulation results, a parametric model of bedrock coherency is calibrated using the plane wave coherency model of Hindy and Novak (1980). Finally, the main results are summarized and discussed, along with comments on their practical applicability, and potential for future research.

2 Stochastic and empirical ground-motion coherency models

Spatial variability of ground motion is caused by a number of factors (Abrahamson et al. 1991b; Der Kiureghian 1996; Zerva and Harada 1997; Somerville et al. 1988) which can be summarized as follows:

a. Differences in the manner of superposition of waves arriving from an extended finite source, and wave scattering by irregularities and inhomogeneity along the wave path and at the site, commonly termed incoherence effects.
b. Traveling-wave or wave-passage effects, in which non vertical waves reach different points on the ground surface at different times, producing a time shift between the motions at those points.

c. Site effects due to the variation in filtering effects of overlying soil columns.

The joint characteristics of stochastic ground motion processes at two locations on the ground surface are fully described by their cross spectral density functions. Such joint characteristics are commonly described by a dimensionless parameter—the so-called coherency function—which is obtained by normalizing the cross spectral density function with the respective power spectral density functions. Considering, motions $a_i(t)$ and $a_j(t)$ at two discrete locations i and j separated by a distance ξ, the complex coherency function in space and circular frequency (ω) is defined as:

$$\gamma_{ij}(\xi,\omega) = \frac{S_{ij}(\xi,\omega)}{\sqrt{S_{ii}(\omega)S_{jj}(\omega)}} \tag{1}$$

where $S_{ij}(\xi,\omega)$ is the smoothed cross spectral density function of $a_i(t)$ and $a_j(t)$; and $S_{ii}(\omega)$ and $S_{jj}(\omega)$ are their smoothed power spectral density functions. Separating $\gamma_{ij}(\xi,\omega)$ into its absolute value and phase, we obtain

$$\gamma_{ij}(\xi,\omega) = \left|\gamma_{ij}(\xi,\omega)\right| \exp\left[i\theta_{ij}(\xi,\omega)\right] \tag{2}$$

where $0 \le \left|\gamma_{ij}(\xi,\omega)\right| \le 1$, is the lagged coherency function and $\theta_{ij}(\xi,\omega)$ is phase spectrum. Lagged coherency squared is called coherency. Generally, lagged coherency decreases with increase in separation distance and frequency.

In this study, all coherencies are computed from simulated time series of ground acceleration; the simulation method is described in the following sections. The simulated time series are aligned to remove wave passage effects (see, for example, Rupakhety and Sigbjörnsson 2012, 2013; Zerva 2009; Ancheta et al. 2011). The alignment is achieved by shifting the time axis of a time series with respect to an arbitrarily selected reference station by an amount corresponding to the time lag where the cross-correlation of the time series and that at the reference station is the maximum. The stationary part of the aligned time series is extracted by visual inspection of the time evolution of Arias Intensity of the simulated time series. A Tukey window with a tapering length of 15 % of the length of the stationary part of the signal was applied. The windowed signals are then used to estimate power and cross spectral density functions which are smoothed. We smooth all power spectra using a Hamming spectral window with a parameter of $M = 39$ ($2M + 1$ is the width of the window). This level of smoothing is selected in order to reduce the variance in lagged coherency. We note that the window length used here is longer than what is reported in Zerva (2009). The fact that the simulated time series in our study have a relatively long duration means that the frequency resolution of the computed spectra is relatively fine. This allows us to use longer windows to effectively reduce variance in computed spectral estimates without seriously compromising their frequency resolution.

Based on coherency estimated from recorded strong motion array data, several models of coherency functions have been proposed in the literature. In the present study, coherencies estimated from simulated ground motion are compared with the model of Hindy and Novak (1980). This model is mathematically expressed as (Novak and Hindy 1979; Hindy and Novak 1980):

$$|\gamma(\xi,\omega)| = \exp\left[-(\alpha\omega\xi)^{\beta}\right] \tag{3}$$

where α and β are model parameters. The dimensionless parameter α is defined as $\alpha = \eta/v_s$, with $\eta = \mu(R/r_o)^{1/2}$, where v_s is the shear wave velocity, R is the distance

travelled by the wave, r_o the scale length of random inhomogeneities along the path, and μ^2 a measure of the relative variation of the elastic properties in medium. The semi-empirical model of Luco and Wong (1986) is a particular case of Eq.(3) with $\beta = 2$. The model has been used extensively by researchers in seismic response analysis of lifelines (e.g. Luco and Wong 1986; Zerva 1994; Der Kiureghian and Neuenhofer 1992). The model is based on shear wave propagation through random media, an approximation that may be valid for the propagation of the waves from the source to the ground surface or from the source to the bedrock-layer interface. Zerva and Harada (1997) and Der Kiureghian (1996) have also used this model for the description of coherency of bedrock motion. Nuti and Vanzi (2004) pointed out that the parameter η has values in the range of 0.02–0.5. The model of Hindy and Novak (1980) is more flexible than the Luco and Wong (1986) model, and is therefore adopted in this study.

3 Ground motion simulation

3.1 Empirical Green's function method

The EGF method of Irikura et al. (1997) considers a rectangular fault plane (length L, width W) divided into $l \times m$ elementary rectangular sub-faults on its surface. Denoting the Green's function associated with a sub-fault (i_o, j_o) by $u_{e_{i_o j_o}}(\mathbf{x}, t)$, the total synthetic signal $U(\mathbf{x}, t)$ at point $\mathbf{x}$ due to the whole fault plane is given by:

$$U(\mathbf{x}, t) = \sum_{i=1}^{l} \sum_{j=1}^{m} \frac{R_s(\theta_{ij}, \varphi_{ij}) r_{i_o j_o}}{R_s(\theta_{i_o j_o}, \varphi_{i_o j_o}) r_{ij}} F(t) * c u_{e_{i_o j_o}}(\mathbf{x}, t) \tag{4}$$

where * denotes convolution. The function $F(t)$ is given by:

$$F(t) = \delta(t - t_{ij}) + \left(\frac{1}{n'}\right)\{1 - \exp(-1)\} \sum_{k=1}^{(n-1)n'} \left[\exp\left\{\frac{-(k-1)}{(n-1)n'}\right\}\right] \times \delta\left(t - t_{ij} - \frac{(k-1)\tau}{(n-1)n'}\right) \tag{5}$$

and t_{ij} is given by Eq. (6):

$$t_{ij} = \frac{r_{ij} - r_o}{v_s} + \frac{\xi_{ij}}{v_r} \tag{6}$$

In these equations, t_{ij} is the phase delay, R_s is the radiation pattern (Aki and Richards 2002), τ is the rise time of the event for which ground motion is being simulated, $r_{i_o j_o}$ is the Euclidean distance between the receiver $\mathbf{x}$ and the rupture starting point on an elementary sub-fault (i_o, j_o), r_{ij} is the Euclidean distance between the receiver and the centre of the sub-fault (i, j), ξ_{ij} is the distance between the hypocentre and the centre of the sub-fault (i, j), v_s is the shear wave velocity, $v_r = 0.72 v_s$ is the rupture velocity, n' is an integer to eliminate spurious periodicity (Irikura 1983), $F(t)$ is the slip-time filtering function, c is the stress drop ratio, r_0 is the Euclidean distance between hypocentre and the receiver, and $\delta(t - t_{ij})$ represents Dirac delta function. The parameters l, m, and n are determined from the scaling relations given by Kanamori and Anderson (1975). For instance, when the seismic moment ratio of the target earthquake (the one being simulated) to the elementary

one (the one used for the empirical Green's function) is N^3, the parameters l, m, and n should each be equal to N (Irikura 1983); the total number of divisions along the length or the width of the fault so that the dimensions of sub-faults are small enough to be treated as point source.

Kamae et al. (1998b) revised the Kanamori and Anderson (1975) relation to allow for the potential difference in stress drop between the target and the small events. The revised relations are:

$$\frac{L}{L_e} = \frac{W}{W_e} = \frac{D}{cD_e} = \frac{\tau}{\tau_e} = \left(\frac{M_0}{cM_{0_e}}\right)^{1/3} = N \tag{7}$$

where L and L_e are fault lengths, W and W_e are widths, τ and τ_e are rise times, and D and D_e are average slip, corresponding to the target event and small event, respectively.

The rise time parameter τ is given by the following relation in Geller (1976):

$$\tau = \frac{16S^{\frac{1}{2}}}{7\pi^{\frac{3}{2}}v_s} \tag{8}$$

where $S = L \times W$ is the fault plane area. Alternatively, the rise time of the target event can be obtained from the similarity equation (Eq. 7) if the rise time of the small event is known (see Irikura 1983).

Because the frequency content of earthquakes is magnitude dependent, direct application of Green's function as in Irikura (1986) can lead to underestimation of ground motion amplitudes at low frequencies. To overcome this, Irikura et al. (1997) introduced the exponential slip function (Eq. 5) (see, for more details, Liang et al. 2006, 2008; Joshi and Midorikawa 2004).

3.2 The Hybrid Green's function method

The HGF method works in a similar way to the EGF method, except that a synthetic time series, rather than recorded time series from small earthquakes, is used as the EGF. In this work, the method of Boore (1983) is used to first simulate ground motion corresponding to an aftershock which is then used as the Green's function to simulate ground motion due to main shocks corresponding to different scenarios. To simulate the Green's function, we calibrate the model parameters of a theoretical Fourier Amplitude Spectrum (FAS) using the aftershock data of the El-Asnam aftershock. Only the S-wave portion of the recorded data is used in calibrating the model. More details on the calibration process and the obtained model parameters are presented in subsequent sections.

The theoretical FAS of ground acceleration shear waves, $A(f)$, at a distance r from a point source with seismic moment M_o is given by (Boore 1983):

$$A(f) = \frac{CM_oS(f,f_c)P(f,f_m)}{r}\exp\left(-\frac{\pi fr}{Q_sv_s}\right) \tag{9}$$

where f is the frequency, Q_s is the shear-wave quality factor accounting for inelastic attenuation,$1/r$ models the geometric spreading, and C is the scaling factor given by Eq. (10):

$$C = \frac{R_s(\theta,\varphi)(FS)(PJ)}{4\pi\rho v_s^3} \tag{10}$$

where $R_s(\theta, \varphi)$ is the radiation pattern of shear waves, FS accounts for free surface, PJ is a factor that accounts for the partitioning of total shear-wave energy into two horizontal components, and ρ is the average density of the rock. The source spectrum $S(f, f_c)$(Brune 1970) is the ω-squared model function of the corner frequency which is given by:

$$f_c = 4.9 \times 10^6 v_s \left(\frac{\Delta\sigma}{M_o}\right)^{\frac{1}{3}} \tag{11}$$

where $\Delta\sigma$ is the stress drop. The function $P(f, f_m)$ is a high-cut filter function with cut-off frequency f_m and is taken from Boore (1983).

4 Case study: Coherency estimated from ground motion simulated using EGF method

The EGF method, which has been used in simulating ground motion at a single location, is extended here to synthesize spatially varying horizontal ground motion at bedrock. The seismic scenario considered is the 10 October 1980 El-Asnam Earthquake of magnitude $M_s = 7.3$, for which ground motion records are not available. The earthquake occurred at 12:25 GMT and the hypocentre was estimated to be at 36°17′N, 1°41′E and at a depth of 12 km (Cisternas et al.1982). The ground motion from the $M_L = 5.6$ aftershock of 08 November 1980 recorded at the Sogedia Factory Station (see Fig. 1) is used as the empirical Green's function. We note that only one aftershock from the source of the target event is available at the study site. In a more favourable situation, if multiple aftershocks

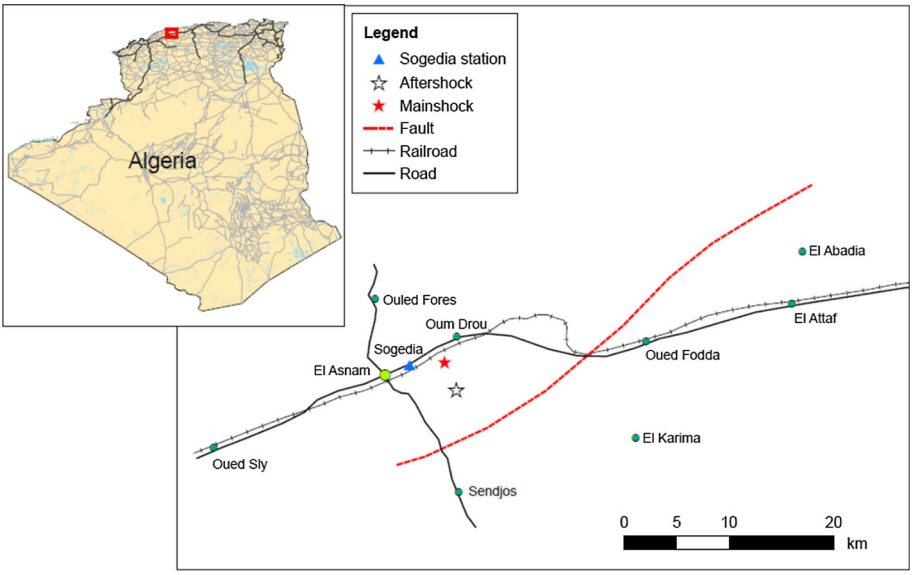

Fig. 1 Map of the epicentral region of the 10 October 1980 El-Asnam Earthquake (simplified from Despeypoux 1984). Epicentral locations (from Cisternas et al. 1982) and the Sogedia Factory station are indicated. The *inset* shows the map of Algeria with the *red rectangle* indicating the location of the epicentral area shown in the main figure

are available, it is preferable to use them as Green's functions from different sections of the source to the site. This allows a more accurate representation of the path effect, especially for large faults. The epicentral distance of this station is about 5 km. The aftershock event took place in the same rupture zone as the mainshock (target) event and with a similar faulting mechanism (Cisternas et al. 1982). In the following, the mainshock, for which ground motion is being simulated, is called the target event, and the aftershock, from which the empirical Green's function is obtained, is called the small event.

In order to simulate ground motion at bedrock, the empirical Green's function should also correspond to the bedrock. Since the bedrock is not outcropping at the recording station, deconvoluted motion (Petrovski and Milutinovic 1981) corresponding to the bedrock is utilized. The time series of the deconvoluted motion is baseline corrected using the method described in Rupakhety et al. (2010). The horizontal components of ground acceleration corresponding to the bedrock are shown in Fig. 2. The fault plane is assumed to be 40 km $\times$ 15 km with a dip angle of 60° (see Fig. 3). Shear wave velocity is taken as 2 km/s (Petrovski and Milutinovic 1981; Yielding et al. 1981) and the corresponding rupture velocity (v_r) is equal to 1.44 km/s. The stress drop of the mainshock is 100 bars (from Dechamps et al. 1982) and, for the small event, a value of 82.57 bars is calculated by using the relation given by Boore (1983) and a corner frequency of 0.37 Hz obtained from a spectral fitting procedure described in Sect. 5. This gives a stress drop ratio (c) equal to 1.21. The fault plane is divided equally into seven parts in both directions, i.e., the scale factor parameter N is equal to 7, and the number n' is taken as 20. The Fourier spectrum (FAS) of the aftershock (see Fig. 6) is characterized by a significant trough around 5 Hz, which yields a rise time of $\tau_e = 0.2$ s; and using the similarity condition (Eq. 7) rise time for the mainshock is estimated to be $\tau = 1.4s$. The latter value is close to the 1s adopted by Dechamps et al. (1982). Other relevant parameters used in the simulation are given in Table 1 in the Appendix. The location of the hypocentre is shown with a red star in Fig. 3, and it lies on cell $(i_0, j_0) = (7, 4)$ from where the rupture is assumed to propagate radially. It is noted that in the presented methodology, the total seismic moment of the target event is assumed to be uniformly distributed over the entire fault plane. This assumption was invoked due to the lack of information on the actual (or expected) slip distribution of the past (or future) event. However, if heterogeneous slip distribution models are available, the methodology can be extended to account for non-uniform slip distribution. This can be done by scaling the contribution of each sub-fault in the total motion in proportion to the seismic moment released at the sub-fault, keeping the total seismic moment unchanged (see, for example, Irikura and Kamae 1994). Horizontal components of ground acceleration are then simulated at five stations at bedrock, namely $S^{(0)}$, $S^{(1)}$, $S^{(2)}$, $S^{(3)}$ and $S^{(4)}$ (see Fig. 3). Station $S^{(0)}$ is considered as the reference station and it lies directly under the Sogedia Factory station; the other stations are separated from it by 40, 100, 200, and

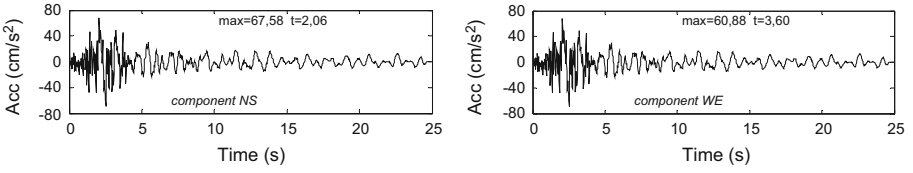

Fig. 2 Acceleration of bedrock (NS and WE component) obtained by deconvolution of ground acceleration due to the 8 November 1980 aftershock recorded at the Sogedia Factory station. The acceleration time series are obtained from Petrovski and Milutinovic (1981)

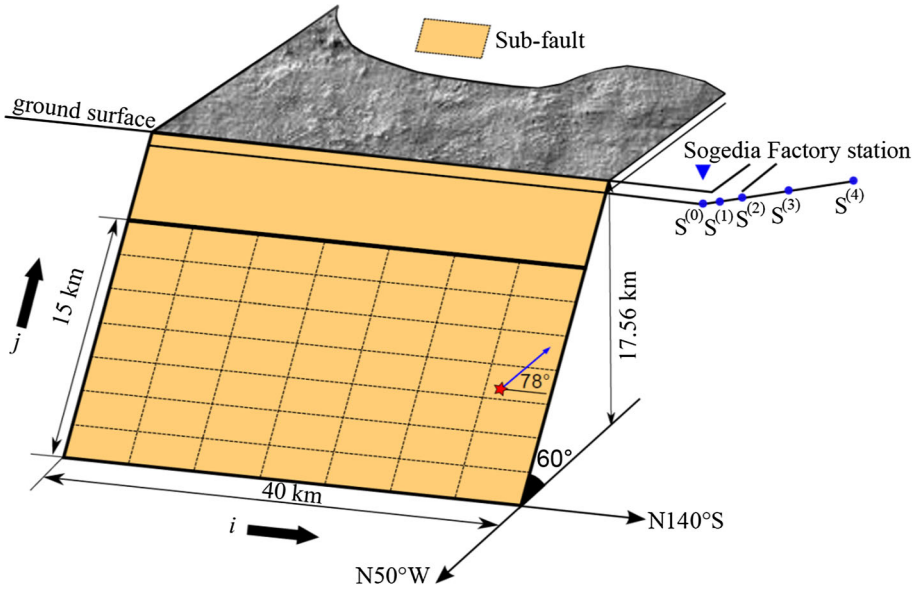

Fig. 3 Schematic representation of the finite-fault model corresponding to the 1980 El-Asnam mainshock; the *star* indicates the location of the hypocentre, the *blue triangle* represents the Sogedia Factory station which recorded the 8 November 1980 aftershock, and the *blue dots* represent the locations of bedrock stations at which ground motion is simulated (dimensions are not to scale). The stations lie on a *line* connecting the Sogedia Factory station to the epicentre

500 m. Epicentral distance of the reference station is 5 km. Simulation of ground motion and estimation of lagged coherencies were performed by computer codes developed by the authors.

The ground acceleration time series simulated at the five stations are shown in Fig. 4. Peak ground acceleration (PGA) of the simulated motion is close to 60 % of acceleration due to gravity. Lagged coherencies computed from the simulated signals are shown in Fig. 5.

The spectral and spatial characteristics of the simulated lagged coherencies, as shown in Fig. 5, are similar to those reported in the literature (see, for example, Zerva 2009). In general, lagged coherency decays in both frequency and space. The lagged coherencies for short separation distances of 40 and 100 m show frequency decays less significant than those for a separation distance of a few hundred meters. It is noted that the coherency estimate for a separation distance of 500 m first decreases with frequency, then starts increasing around 7 Hz. Such apparent increase of coherency with frequency is physically not meaningful and is most likely due to uncertainties in the spectral estimation and smoothing operation (see Zerva 2009 and Rupakhety and Sigbjörnsson 2012 for a more detailed discussion). The coherency is significantly less than 1.0 at low frequencies (1–2 Hz) for the long station separation of 500 m and at intermediate frequencies (3–5 Hz) for the medium separation distance of 200 m. Such loss in coherency has been attributed to (see, for example, Zerva 2009) scattering of waves along the propagation path (caused by heterogeneities in the path) and near the stations (due to heterogeneities near the surface). It is noted that such effects are not fully modelled in the present simulation method because EGF is available at only one station. In this sense, spatial variation of scattering effects is not captured in the simulation.

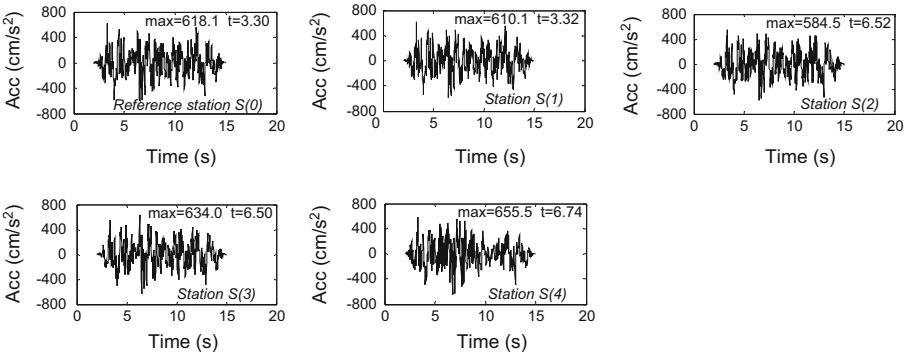

Fig. 4 Transverse (orthogonal to the epicentral direction) component of ground acceleration simulated at the five stations. The simulated signals are first aligned to eliminate wave passage effects. Stationary part (by visual inspection of time evolution of Arias Intensity) is then extracted and tapered with Tukey windows with end taper length equal to 15 % of the length of the signal. These tapered signals are used to compute lagged coherencies shown in Fig. 5

Fig. 5 Lagged coherencies at the four stations obtained from ground acceleration time series shown in Fig. 4

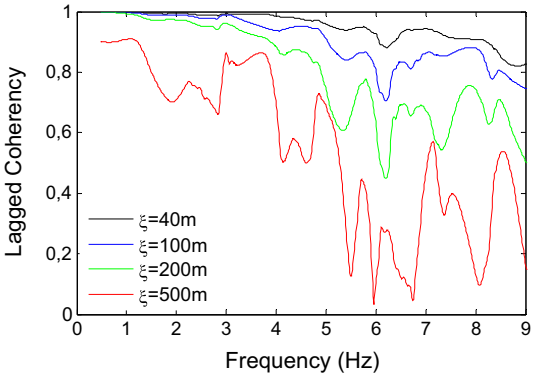

The relatively small value of coherence at low frequencies and large separate distance may therefore be due to source effects in the near field, which is found to be prominent at low frequencies (Abrahamson et al. 1991a). This behaviour can also be explained by the fact that the term t_{ij} in Eq. (6) might become nearly random in the near-field region of a rectangular fault plane (Irikura 1986) and consequently the phase difference between two stations increases with increasing separation distances. In the far-field, the source to site distance is large compared to the inter-station separation distance of a few hundred meters, and therefore loss of coherence with separation distance is less pronounced than that in the near-field, as the term t_{ij} is almost the same for the different stations.

The results of the simulations indicate that source effects in coherency are significant; considerable loss in coherency is obtained just by modelling the source effect. On the other hand, the source effects, site effects, and scattering effects may constructively and destructively interfere in coherency decay (see Zerva 2009 for a detailed discussion), and isolating these different effects from recorded data is not straightforward. The simulation method presented in this work models coherency decay mainly due to source effect, which seems significant for the case under study.

5 Sensitivity analysis of simulated coherency

It is well known that the coherency of ground motion is affected by seismic source, propagating medium, site condition, the relative orientation between source and site (directivity) and parameters such as fault orientation and fault depth (Jin et al. 2000; Ding et al. 2004; Ding and Song 2010; Santa-Cruz et al. 2000; Schneider et al. 1992; Somerville et al. 1988, 1991; Zerva and Shinozuka 1991; Abrahamson et al. 1991a; Horike and Takeuchi 1996). The sensitivity of ground motion parameters at a station simulated by the EGF method has been studied by Pavic et al. (2000). However, the sensitivity of coherency of simulated ground motion to the parameters used in simulation has not been studied. In this section, such a sensitivity analysis is presented. The main objective of this analysis is to identify those simulation parameters which have a large influence on simulated coherency functions, and therefore need to be well constrained for the simulation of the strong ground motion field (Zerva 1994; Jin et al. 2000; Hao et al. 1989). The parameters considered in this analysis are magnitude (source parameter), wave velocity (path parameter) and epicentral distance (path parameter). It is noted that other source phenomena, such as heterogeneous slip distribution, directivity effect, and focal mechanism can influence the coherency of the resulting ground motion. Parameters such as slip distribution and the directivity effect are not easily modelled (or predicted for future events). In this sense, priority is given to those source parameters which are relatively well understood in the sensitivity analysis presented in this work. The effects of other relevant source parameters are outside the scope of this study, but parametric studies investigating such effects could shed more light on source effects in coherency of ground motion in the near-fault and are currently under investigation. Because EGFs corresponding to various scenarios of these parameters are not available, we use the HGF method for ground motion simulation.

The stress-drop ratio is assumed to be 1. We also note that we investigated the effect of this parameter in coherency estimates and decided that a value equal to 1 was suitable. It was found that, although this parameter has some effects in the simulated ground motion amplitudes, lagged coherencies were not very sensitive to this parameter. A direct implication of changing this parameter is the change in number of sub-faults to be used in simulation. If too few sub-faults are used (corresponding to large values of c), the finite-fault effect is not appropriately modelled. However, such a situation is not likely because, within reasonable variations of the parameter, the number of sub-faults remains unchanged (see Eq. 7) as it is rounded off to the next integer. When a suitable value of number of sub-faults is selected, c needs to be adjusted to conserve the seismic moment. The simulated coherency functions were found to be relatively insensitive to the choice of this parameter as long as a reasonable number of sub-faults is used in the simulation. The EGFs are simulated using the stochastic method with a theoretical source spectrum given by Eq. (9).

Some parameters of the spectrum are kept constant for all scenarios, namely: $FS = 2$, $PJ = 0.71$ and $\Delta\sigma = 100$ bars (from Dechamps et al. 1982). The parameters Q_s, f_c and f_m were obtained by fitting the theoretical source spectral model of Eq. (9) to the FAS of the deconvoluted aftershock ground motion time series recorded at the Sogedia Factory station. Only the shear wave parts of the two horizontal components of motion were extracted and windowed. Rotation-invariant estimate of FAS of horizontal motion is then obtained based on the formulation presented in Rupakhety and Sigbjörnsson (Rupakhety and Sigbjörnsson 2014a, b). The FAS is fitted to the theoretical model yielding $Q_s = 45$, $f_c = 0.37$ Hz and cut-off frequency, $f_m = 20$ Hz. Figure 6 shows a comparison between the

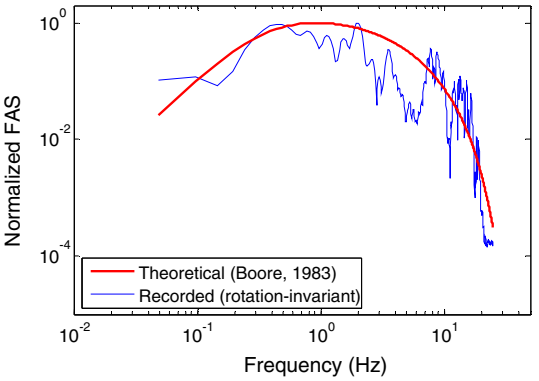

Fig. 6 Comparison between the recorded and theoretical FAS (normalized by its maximum) of ground acceleration at bedrock. The recorded spectrum is from 8 November 1980 aftershock at Sogedia Factory station deconvoluted at bedrock (see text above for more details). The hypocentral distance is 12.96 km, and an average radiation pattern of 0.868 is used

rotation invariant spectra and the theoretical model fitted to it. The other parameters required for simulating EGF are mentioned in the following sections as they depend on the different scenarios being simulated. Using the FAS spectra and phase spectrum obtained from the aftershock record, EGF are simulated using the stochastic method. These EGFs are then used to simulate ground acceleration at the five bedrock stations. Coherency estimates are obtained from the simulated ground motion using the procedure described in Sect. 2.

5.1 Effect of shear wave velocity

Shear wave velocity and rupture velocity, which are closely related, play an important role in how the seismic waves radiated from the different sections of an extended source superimpose in time at a station. Since the superposition of these waves at nearby stations is expected to affect the coherency of motion across the stations, we study the sensitivity of coherency to shear wave velocity. Three different scenarios of generic rock with $v_s^a = 1500$ m/s, $v_s^b = 2500$ m/s, and $v_s^c = 3500$ m/s are considered to simulate ground acceleration at the five stations using the HGF method. Table 2 in the Appendix lists the others relevant properties of the generic rocks (from Betbeder-Matibet and Bour 2002; Chapellier and Mari 2011).

Lagged coherencies corresponding to the transverse component of ground acceleration for the three generic rocks are shown in Fig. 7. The results indicate that at low frequencies (<2 Hz) lagged coherency is not very sensitive to shear wave velocity. At such low frequencies, the wavelengths of shear waves are not as sensitive to variations in wave velocity as they are at high frequencies. High sensitivity of wavelengths might result in high sensitivity of coherence within a small spatial area. It is also observed that the decay of coherency with frequency is faster when the shear wave velocity is lower. At frequencies above 2 Hz, the coherency seems, in general, to increase with shear wave velocity, except for a separation distance of 500 m, where the increase is not consistent for all frequencies. The overall increase of coherency with shear wave velocity is expected from the fact that the differential arrival time of shear waves radiated from different sections of the fault decreases with increasing wave velocity. Increasing wave velocity also implies smaller time difference in arrival of waves radiated from a sub-fault at different stations, which results in higher coherency. It should be noted that the simulation method used here considers only the source effect in loss of coherency and does not take into

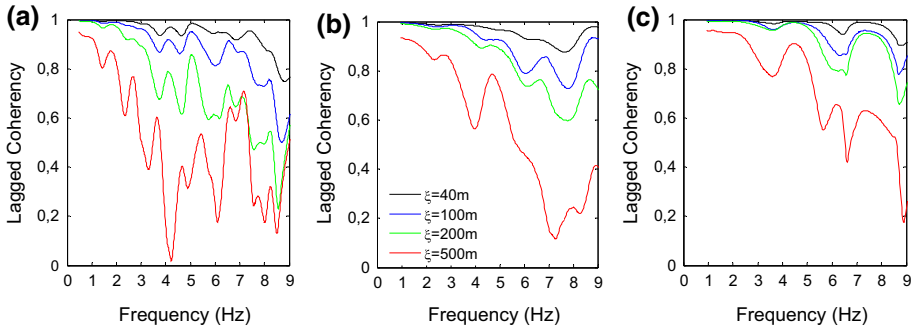

Fig. 7 Lagged coherencies of transverse ground acceleration for three generic rocks: **a** for $v_s^a = 1500$ m/s, **b** for $v_s^b = 2500$ m/s, and **c** for $v_s^c = 3500$ m/s. The *black*, *blue*, *green*, and *redlines* correspond to separation distance of 40, 100, 200, and 500 m, respectively

account scattering effects in the propagation medium or near the receiver. Even in lack of these scattering effects, considerable loss in coherency is observed at medium and high frequencies, which implies that source effects alone can have a significant effect on coherency. This effect is expected to be more pronounced in the near-field region (see, Abrahamson et al. 1991a; Ding et al. 2004)—which is the case of the present analysis—for the reasons explained in Sect. 4.

5.2 Effect of earthquake magnitude

Abrahamson et al. (1991a) show some evidence of magnitude dependence of coherency. At frequencies below 5 Hz small magnitude events tend to have lower coherency than large magnitude events, while at frequencies of 6–10 Hz, the reverse is true. Somerville et al. (1988) suggested that coherency for aftershocks is greater at all frequencies than that for mainshock in the near-field.

To study the effect of the magnitude on bedrock coherency, we compute accelerograms which correspond to two earthquake events. One of them corresponds to the 1980 El-Asnam mainshock with $M_s = 7.3\,(M_0 = 540 \times 10^{24}$ dyne - cm) and the other one corresponds to the 13 May 1995 Kozani-Greneva Earthquake with $M_w = 6.5\,(M_0 = 55 \times 10^{24}$ dyne - cm) which occurred in northwestern Greece. The five receiver stations are placed on bedrock of type b (shear wave velocity equal to 2500 m/s) for both events. For the larger event, simulations are based on the HGF method using aftershock data from 8 Nov 1980 aftershock. The fault geometry is considered to be the same as that of the El-Asnam Earthquake, with $N = 7$ and $(i_0, j_0) = (7, 4)$. For the smaller event, the HGFs are simulated from the recording of the largest aftershock of the Kozani-Greneva Earthquake that occurred on 15 May 1995 with $M_w = 5.1\,(M_0 = 0.44 \times 10^{24}$ dyne - cm). For this event, a rectangular fault with dimensions 29 km $\times$ 13 km is divided into 5×5 sub-faults. The strike, dip, and rake of this event are taken to be the same as that of the El-Asnam mainshock. The cut-off frequency is taken to be 7 Hz and the stress-drop 12.19 bars. The relevant parameters of this event are taken from Roumelioti et al. (2000). The rupture is assumed to start at the cell $(i_0, j_0) = (1, 2)$ with radial propagation. The resulting lagged coherency functions are shown in Fig. 8. It is observed that coherency of the smaller earthquake is larger than that of the larger one at all frequencies, which is consistent with

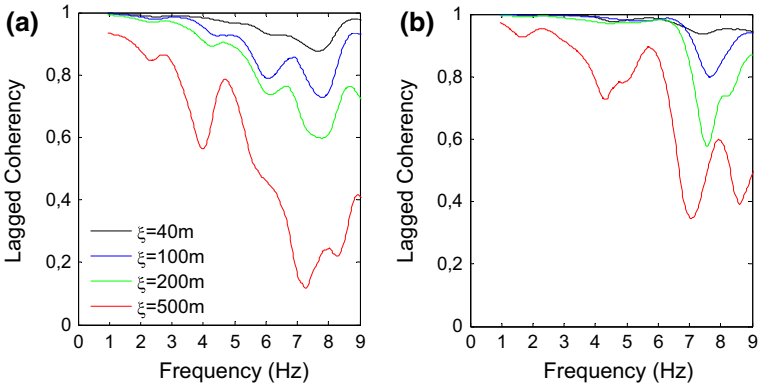

Fig. 8 Lagged coherency at bedrock for **a** large magnitude and **b** and small magnitude earthquakes. The *black*, *blue*, *green*, and *red lines* represent separation distance of 40, 100, 200, and 500 m, respectively

the observations of Somerville et al. (1988). For the smaller earthquake, and for a separation distance up to 200 m, loss in coherency does not start until about 6 Hz, whereas lagged coherency for the 500 m separation distance steadily decreases from about 1 Hz. On the contrary, loss in coherency with frequency starts at much lower frequencies for all separation distances for the larger earthquake. Spatial decay of lagged coherency is more pronounced for the larger earthquake. These results indicate the finite source effect on lagged coherency. As the rupture area increases, seismic waves radiated from different parts of the fault arrive more asynchronously at nearby stations, resulting in loss of coherency.

5.3 Effect of epicentral distance

Abrahamson et al. (1991a), using data recorded on soil site at the LSST array in Lotung, Taiwan, observed that coherency in the near-field was lower than that in the far-field at low frequencies, which was interpreted as a source effect. Whereas the reverse was true for higher frequencies, which was interpreted as a path effect. Similar results were found by Somerville et al. (1988). In the presented simulation method, site effects are not modelled and, thus, the loss in coherency is mainly due to the source effect. This section investigates the importance of this effect for different epicentral distances.

Three different epicentral distances are considered: $d_1 = 5$ km, $d_2 = 33$ km, and $d_3 = 65$ km, which correspond, respectively, to hypocentral distances of 12.96, 35.1, and 66.09 km. These three distances are assumed to represent, for the 1980 El-Esnam mainshock, the near-, intermediate-, and far-field (see Hammoutene et al. 1992). By using the HGF method, ground acceleration time series are simulated at three sets of five stations on bedrock of type b. On each set, the reference stations are placed at the epicentral distance mentioned above, and the other stations are separated from it by 40, 100, 200, and 500 m. All the stations on the hanging wall and lie on the radial line from the epicentre of the target event to the Sogedia Factory station. HGFs for the simulation are based on the $M_L = 5.6\,(M_0 = 1.55 \times 10^{24}$ dyne $-$ cm) event.

Figure 9 presents the lagged coherency functions at different separation distance in the near-, intermediate-, and far-field. It can be observed that lagged coherency increases at all frequencies with epicentral distance. In the far-field, and on bedrock, the loss in coherency

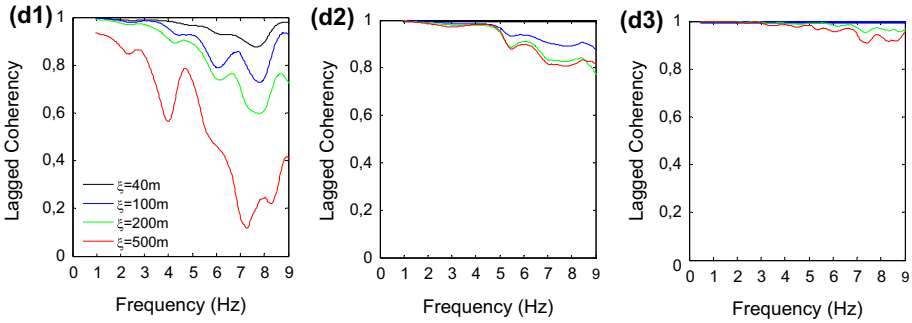

Fig. 9 Lagged coherency functions, from left to right, corresponding to near-, intermediate-, and far-field of the 1980 El-Esnam Earthquake. The *black*, *blue*, *green*, and *red lines* correspond to separation distance of 40, 100, 200, and 500 m, respectively

is negligible up to 8 Hz. This is expected because the simulation method presented here only accounts for the source effect, which is not strong in the far-field. It can thus be concluded that the effect of finite source in lagged coherency is negligible in the far-field, which implies that scattering and local site effects are the main sources of incoherence. In the near-field, however, considerable loss in coherency is observed, which indicates that source effects are important. In the near-field, the term t_{ij} in Eq. (6) is sensitive to the separation distance between the stations, which implies asynchrony in arrival of waves radiated from different sub-faults at these stations. This asynchrony results in loss of coherency. In the far-field, this term is not sensitive to inter-station separation distance and, therefore waves radiated from different stations arrive almost synchronously at nearby stations. This results in highly coherent motion. The consequence of this differential sensitivity is also apparent from Fig. 9, where lagged coherency functions are less sensitive as epicentral distance increases . A word of caution regarding this interpretation is that the presented results account only for finite source effects, and lack modelling of scattering and local site effects. When these effects are present, lagged coherencies in the far-field are expected to be smaller than what is presented in Fig. 9.

In summary, a finite source produces more incoherent motion than a point source, as is suggested by Faccioli (1991). In the near-field of an extended seismic source, ray paths extending from different portions of the ruptured fault give rise to differential ground motion at two points some distance apart because of different azimuths, incidence angles, attenuation, and scattering paths.

6 Parametric modelling of spatial coherency

In this section, we calibrate a parametric model to the coherency functions computed from simulated ground motion corresponding to the 1980 El-Esnam Earthquake (see Sect. 4, and Fig. 5). The functional form of the model is taken to be the same as that of Hindy and Novak (1980), as presented in Eq. (3). This model was selected because it has been extensively used by researchers in seismic response analysis of lifelines. Since this model does not explicitly consider scattering effects and noise, it is often viewed as a plane wave coherency model and is, therefore, suitable for our analysis. Ramadan and Novak (1993) found that the exponentially decaying spatial incoherence model of Hindy and Novak

(1980) is in general agreement with a number of spatial incoherence expressions when the model parameters are chosen appropriately. We note that we tried to calibrate the Harichandran and Vanmarcke (1986) model without success, as this model did not seem to be well constrained by the simulated coherency data. The model of Luco and Wong (1986), which constrains the parameter β of the Hindy and Novak (1980) model to 2, was found to be too restrictive and less applicable in space-frequency decay of lagged coherencies. To calibrate the parameters of the Hindy and Novak (1980) model, we use non-linear least squares regression in the hyperbolic arctangent $\left(\tanh^{-1}\right)$ transformation of lagged coherency. Such a transformation is preferable because the transformed variable has approximately frequency independent variance (Jenkins and Watts 1969). The frequency and separation distance ranges used fitting the model were $[0-8]$ Hz and $[0-500]$ m, respectively. The regression parameters were found to be $\alpha = 5.87 \times 10^{-5}$ and $\beta = 1.52$. The R-squared value of the fit was found to be 0.88 with a root mean square error of 0.30, which demonstrate the goodness of fit of the model. A comparison between lagged coherencies and the fitted model is shown in Fig. 10.

The comparison in Fig. 10 shows that the model fits the simulated lagged coherencies relatively well for separation distances up to 100 m. For separation distance of 100 m, the fit is good up to a frequency of 5 Hz. For a separation distance of 500 m, the model fits simulation results relatively well and, therefore, the model is considered to capture the overall spatial and spectral characteristics of lagged coherency. The quality of fit is also clear from the residuals (difference between model prediction and simulated results) in $\tanh^{-1}$ transformation as shown in Fig. 11. The mean value of the residuals is closest to 0 for a separation distance of 100 m, while it is most biased for a separation distance of 500 m.

7 Summary and Conclusions

The main contribution of this work is to present an approach to simulate spatially variable ground motion using the EGF method. This method has been extensively used in the literature to simulate point estimates of strong ground motion. In this work, we test whether it is suitable for simulating a ground motion field within a relatively small spatial extent,

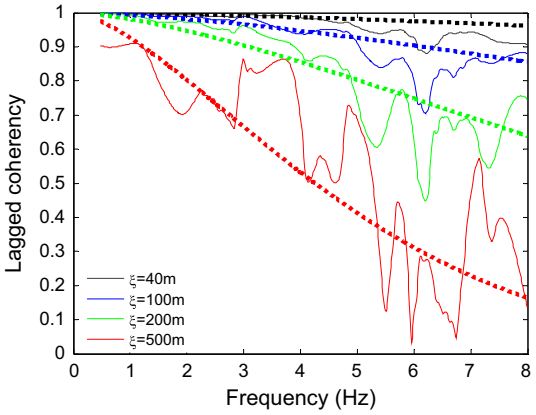

Fig. 10 Lagged coherencies of transverse ground acceleration at bedrock (see Fig. 5) due to the 1980 El-Asnam Earthquake (*solid lines*) and the corresponding Hindy and Novak (1980) model (*dashed lines*)

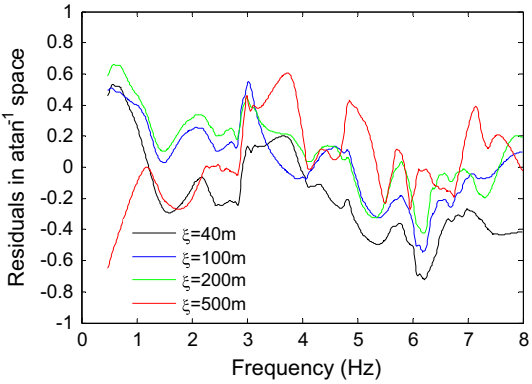

Fig. 11 Residual $\tanh^{-1}$ lagged coherencies corresponding to the simulated results and fitted model shown in Fig. 10

thereby modelling incoherence effects. The case study and parametric study presented herein suggest that the presented approach is suitable for simulating incoherence due to the finite source effect. In particular, plane wave coherency estimates can be obtained through such simulations. Although loss in coherency is due to source, scattering, and local site effects, the present methodology captures only the effect of the finite source. This is a limitation of the method. Nevertheless, in absence of recorded data, the method can be useful in modelling spatially variable ground motion, in the sense that the simulated coherencies can be considered as upper bounds of what is expected in the presence of scattering and local site effects. It needs to be pointed out that further research in incorporating these effects in simulated lagged coherencies is underway. Of special interest here is the development of models to convert lagged coherencies at bedrock to those at the surface of a random soil layer. In addition, investigation of scattering effects will also be valuable. In the practical sense, and in absence of strong motion array data in the study region, the results presented herein could provide a rough approximation of ground motion coherency, which can be used in (a) random vibration analysis of lifeline structures, or (b) simulating spatially variable ground motion for time history analysis of such structures. To facilitate such modelling, a parametric model of lagged incoherency has been presented. The parametric model follows the same functional form as that of Hindy and Novak (1980) and the model parameters are calibrated using simulated lagged coherency functions. Due to the lack of scattering effects in the simulated ground motion, the presented model should be considered representative of plane wave coherence, as is the case of the Hindy and Novak (1980) model.

A parametric study investigating the sensitivity of lagged coherency showed that shear wave velocity, earthquake magnitude, and epicentral distance are all important factors that contribute to plane wave coherency. Larger shear wave velocity was found to produce more coherent motion in general. Larger earthquakes were found to produce more incoherent motion. In the near-field, the finite source effect seems to be significant, producing incoherent motion, while in the far-field, plane wave coherency was found to be almost equal to one up to a frequency of 8 Hz. Because structures in the near-field are more severely affected by earthquakes, the practical significance of the presented methodology is justified in the sense that it provides at least a first approximation, and possibly an upper bound, on lagged coherencies.

Further study on the effects of other relevant parameters such as, geometry of the fault, location of stations on the hanging or foot wall, directivity of stations with respect to

rupture propagation, and geometry of the rupture source will be valuable in understanding their effects in plane wave coherency. For example, randomness in rupture velocity and rise time on the fault can enrich the frequency content of ground motion (Zerva and Shinozuka 1991). The effects of fault geometry and size of sub-events could also have significant effects on ground-motion coherency (see, for example, Ding and Song 2010). Bilateral rupture propagation and source directivity effects can also influence ground-motion coherency (see, Spudich 1994). Source asperities may generate highly coherent energy in a narrow frequency band (Abrahamson et al. 1991a) thereby altering the spectral nature of lagged coherency functions. These effects, among others, need to be investigated in detail, preferably using well-recorded, past earthquakes. Furthermore, effects of layered soil (see, for example, AfifChaouch et al. 2014) and scattering effects need to be investigated.

Appendix

See Tables 1 and 2.

Table 1 Input parameters for the application of the EGF method

Parameter	Simulation of the El-Asnam mainshock		
	Target event	Small event	
M_s	7.3	5.6	
$M_0(dyne.cm)$	540×10^{24} from Dechamps and Gaudemer (1981)	1.55×10^{24} estimated from the Bolt and Herraiz (Bolt and Herraiz 1983) equation: $\log M_0 = (17.92 \pm 1.02) + (1.11 \pm 0.15)M_L$ *for* $3 \leq M_L \leq 6.2$	
Epicenter coordinates	36°17 N 01°41E	36°14 N 01°40E	
Hypocentral depth (km)	12	12	
Strike angle (°)	220 Calculted by Dechamps and Gaudemer (1981)	220	
Dip angle (°)	60	60	
Rake angle (°)	78	78	
Fault length (km)	40	5.714	From scaling relations: Eq. (7)
Fault width (km)	15	2.142	
Rise time τ (s)	1.4	0.2	
Coordinates of the reference station point $S^{(0)}$			
Hypocentral distance $r_{i_0 j_0}(km)$	12.96		
Radiation pattern $R_s(\theta_{i_0 j_0}, \varphi_{i_0 j_0})$	0.868		

Table 2 Geotechnical characteristics of generic rocks used in parametric study (Petrovski and Milutinovic 1981; Yielding et al. 1981; Betbeder-Matibet and Bour 2002; Chapellier and Mari 2011)

Rock type	Sogedia El-Asnam	Medium (a)	Hard (b)	Very hard (c)
ρ (density)	2.4 gr/cm^3	2.2	2.5	2.8
Vs (*S*-wave velocity)	2000 m/s	1500	2500	3500
Vp (*P*-wave velocity)	3460 m/s	3100	4500	5300
Qs (Quality factor)	45	125	230	300

References

Aagaard BT, Graves RW, Rodgers A, Brocher TM, Simpson RW, Dreger D, Petersson NA, Larsen SC, Ma S, Jachens RC (2010) Ground-motion modelling of Hayward fault scenario earthquakes, part II: simulation of long-period and broadband ground motions. Bull Seismol Soc Am 100:2945–2977

Abrahamson N, Schneider JF, Stepp JC (1991a) Spatial coherency of shear waves from the Lotung, Taiwan large-scale seismic test. Struct Saf 10:145–162

Abrahamson N, Schneider JF, Stepp JC (1991b) Empirical spatial coherency functions for application to soil-structure interaction analyses. Earthq Spectra 7(1):1–27

Afif Chaouch K, Tiliouine B, Hammoutene M (2014) Effects of layered stochastic soil profile on the coherency functions of spatially variable seismic ground motions: case study of the El-Asnam region (NW Algeria). In Proceedings of the 8th European Conference on numerical methods in geotechnical engineering: probabilistic methods and neural networks, vol 2, pp 441–446

Aki K, Richards PG (2002) Quantitative seismology, 2nd edn. University Science Books, Sausalito

Ancheta TD, Stewart JP, Abrahamson NA (2011) Engineering characterization of earthquake ground motion coherency and amplitude variablity. In: 4th IASPEI/IAEE international symposium: effects of surface geology on seismic motion. University of California Santa Barbara, 23–26 Aug 2011

Betbeder-Matibet J, Bour M (2002) Lois d'atténuation pour les valeurs du pic du mouvement et d'ordonnées spectrales. Cahier Technique AFPS 23:23–56

Bi K, Hao H (2012) Modelling and simulation of spatially varying earthquake ground motions at sites with varying conditions. Probab Eng Mech 29:92–104

Bielak J, Ghattas O, Kim EJ (2005) Parallel octree-based finite element method for large-scale earthquake ground motion simulation. Comput Model Eng Sci 10:99–112

Bielak J, Graves RW, Olsen KB, Taborda R, Ramirez-Guzman L, Day SM, Ely GP, Roten D, Jordan TH, Maechling PJ, Urbanic J, Cui Y, Juve G (2010) the shakeout earthquake scenario: verification of three simulation sets. Geophys J Int 180:375–404

Bolt BA, Herraiz M (1983) Simplified estimation of seismic moment from seismograms. Bull Seismol Soc Am 73:735–748

Boore DM (1983) Stochastic simulation of high-frequency ground motions based on seismological models of the radiated spectra. Bull Seismol Soc Am 73:1865–1894

Boore DM (2003) Simulation of ground motion using the stochastic method. Pure appl Geophys 160:635–676

Boore DM, Atkinson GM (1987) Stochastic prediction of ground motion and spectral response parameters at hard-rock sites in Eastern North America. Bull Seismol Soc Am 72:440–467

Brune JN (1970) Tectonic stress and the spectra of seismic shear waves from earthquakes. J Geophys Res 75:4997–5009

Chapellier D, Mari JL (2011) Cours de géophysique, Université de Lausanne. Institut français du pétrole

Cisternas A, Dorel J, Gaulon R (1982) Models of the complex source of the El-Asnam Earthquake. Bull Seismol Soc Am 72:2245–2266

Dechamps A, Gaudemer Y (1981) Etude d'ondes telesismiques longues périodes. Journées Scientifiques d'Alger sur le séisme d'El-Asnam du 10 Octobre 1980, 15 et 16 Juin: 132–138

Dechamps A, Gaudemer Y, Cisternas A (1982) The El-Asnam, Algeria, earthquake of 10 october 1980: multiple-source mechanism determined from long-period records. Bull Seismol Soc Am 72:1111–1128

Der Kiureghian A (1996) A coherency model for spatially varying ground motions. Earthq Eng Struct Dyn 25:99–111

Der Kiureghian A, Neuenhofer A (1992) Response spectrum method for multiple support seismic excitation. Earthq Eng Struct Dyn 21:713–740

Despeypoux (1984) Some lessons to be drawn from the El-Asnam Earthquake of 10 October 1980. In Proceedings of the 8th world conference earthquake engineering V, San Francisco, California, USA, pp 849–856
Ding H, Song Z (2010) Effects of source parameters on coherency function of ground motion. J Vib Shock 29(7):16–18
Ding H, Liu Q, Jin X, Yuan Y (2004) Coherency function model of ground motion at base-rock. In Proceedings of the 14th world conference earthquake engineering, paper no. 2692, Vancouver, BC, Canada
Faccioli E (1991) Studies on the spatial variability of ground motion for the design of extended structures. In: International workshop on seismology and earthquake engineering, Mexico, pp 177–186
Faccioli E, Maggio F, Paolucci R, Quarteroni A (1997) 2D and 3D elastic wave propagation by a pseudo-spectral domain decomposition method. J Seismol 1:237–251
Geller RJ (1976) Scaling relations for earthquake source parameters and magnitudes. Bull Seismol Soc Am 66:1521–1523
Graves RW (1996) Simulating seismic wave propagation in 3D elastic media using staggered-grid finite differences. Bull Seismol Soc Am 86:1091–1106
Graves RW, Pitarka A (2010) Broadband ground-motion simulation using a hybrid approach. Bull Seismol Soc Am 100:2095–2123
Hadley DM, Helmberger DV (1980) Simulation of strong ground motions. Bull Seismol Soc Am 70:617–630
Hammoutene M, Tiliouine B, Bard PY (1992) A two dimensional nonstationary optimized accelerogram scaled for magnitude, distance and soil conditions. In Proceedings of the 10th world conference earthquake engineering, vol 2, pp 817–821, Madrid, Spain
Hao H, Gaull BA (2004) Prediction of seismic ground motion in Perth Wester Australia for engineering application. In: 13th world conference earthquake engineering, paper no. 1892, Vancouver, BC, Canada
Hao H, Oliveira CS, Penzien J (1989) Multiple-station ground motion progressing and simulation based on SMART-1 array data. Nucl Eng Des 111:293–310
Harichandran RS, Vanmarcke E (1986) Stochastic variation of earthquake ground motion in space and time. J Eng Mech ASCE 112(2):914–925
Harichandran RS, Wang W (1990) Response of indeterminate two span beam to spatially varying earthquake excitation. Earthq Eng Struct Dyn 19:173–187
Hartzell SH (1978) Earthquake aftershocks as Green functions. Geophys Res Lett 5:1–4
Hindy A, Novak M (1980) Pipeline response to random ground motion. J Eng Mech ASCE 106(2):339–360
Horike M, Takeuchi Y (1996) Comparison of spatial variation of seismic motion in three different geological conditions. In Proceeding of the 11th world conference earthquake engineering, paper no. 135, Acapulco, Mexico
Irikura K (1983) Semi empirical estimation of strong ground motions during large earthquakes. Bull Disaster Prev Res Inst Kyoto Univ Jpn 33:63–104
Irikura K (1986) Prediction of strong acceleration motions using empirical Green's function. In: Proceedings of the 7th Japan Earthquake Engineering Symposium, vol 7, pp 151–156
Irikura K, Kamae K (1994) Estimation of strong ground motion in broad-frequency band based on a seismic source scaling model and an empirical Greens function technique. Ann Geophys XXXVII(6): 1721–1743
Irikura K, Muramatu I (1982) Synthesis of strong ground motions from large earthquakes using observed seismograms of small events. In: Proceedings of the 3rd international microzonation conference, Seattle, pp 447–458
Irikura K, Kagawa T, Sekiguchi H (1997) Revision of the empirical Green's function method by Irikura (1986), programme and abstracts. The Seismological Society of Japan, vol 2, p B25
Jenkins GW, Watts DG (1969) Spectral analysis and its applications. Holden Day, San Francisco
Jin X, Chen C, Mi-yu Zhang (2000) Far-field analysis of effects of unilateral rupturing fault on the space correlation of strong ground motion. Acta Seismol Sin 13(5):544–551
Joshi A, Midorikawa S (2004) A simplified method for simulation of strong ground motion using finite rupture model of the earthquake source. J Seismol 8:467–484
Joshi A, Mohan K (2008) Simulation of accelerograms from simplified deterministic approach for the 23rd October 2004 Niigata-ken Chuetsu, Japan earthquake. J Seismol 12:35–51
Kamae K, Irikura K (1998) Source model of the 1995 Hyogoken Nanbu earthquake and simulation of near source ground motion. Bull Seismol Soc Am 88:400–412
Kamae K, Irikura K, Pitarka A (1998a) A technique for simulating strong ground motion using hybrid Green's function. Bull Seismol Soc Am 88:357–367

Kamae K, Bard PY, Irikura K (1998b) Prediction of strong ground motion at EURO-SEISTEST site using the empirical Green's function method. J Seismol 2:193–207
Kanamori H (1979) A semi empirical approach to prediction of long period ground motions from great earthquakes. Bull Seismol Soc Am 69:1645–1670
Kanamori H, Anderson DL (1975) Theoretical basis of some empirical relations in seismology. Bull Seismol Soc Am 65:1073–1095
Komatitsch D, Vilotte J-P (1998) The spectral element method: an efficient tool to simulate the seismic response of 2D and 3D geological structures. Bull Seismol Soc Am 88(2):268–392
Liang JZ, Hao H, Gaull BA, Sinadinovski C (2006) Simulation of strong motions with a combined Grenn's function and stochastic approach. Earthquake Engineering in Australia, Canberra, 24–26 Nov 2006
Liang JZ, Hao H, Gaull BA, Sinadinovski C (2008) Estimation of strong ground motions in Southwest Western Australia with a combined Green's function and stochastic approach. J Earthq Eng 12(3):382–405
Luco JE, Wong HL (1986) Response of a rigid foundation to a spatially random ground motion. Earthq Eng Struct Dyn 14:891–908
Lupoi A, Franchin P, Pinto PE, Monti G (2005) Seismic design of bridges accounting for spatial variability of ground motion. Earthq Eng Struct Dyn 34:327–348
Mai PM, Imperatori W, Olsen KB (2010) Hybrid broadband ground-motion simulations: combining long-period deterministic synthetics with high-frequency multiple S-to-S backscattering. Bull Seismol Soc Am 100:2124–2142
Mazzieri I, Stupazzini M, Guidotti R, Smerzini C (2013) SPEED: spectral elements in elastodynamics with discontinuous Galerkin: a con-conforming approach for 3D multi-scale problems. Int J Numer Methods Eng 95(12):991–1010
Menke W, Lerner Lam AL, Dubendorff B, Pacheco J (1990) Polarization and coherence of 5 to 30 Hz seismic wave fields at a hard rock site and their relevance to velocity heterogeneities in the crust. Bull Seismol Soc Am 80:430–449
Mikumo T, Irikura K, Imagawa K (1981) Near field strong motion synthesis from foreshock and aftershock records and rupture process of the main shock fault (abs.). IASPEI 21st General Assembly, London
Nazmy AS, Abdel-Ghaffar AM (1992) Effects of ground motion spatial variability on the response of cable-stayed bridge. Earthq Eng Struct Dyn 21:1–20
Novak M, Hindy A (1979) Seismic response of buried pipelines. In: Proceedings of the third Canadian conference on earthquake engineering, Montreal, Canada, Jun, vol 1, pp 177–203
Nuti C, Vanzi I (2004) Influence of earthquake spatial variability on the differential displacement of soil and single degree of freedom structures. Technical Report DIS 1/2004, Departement of Structures, University of Roma Tre
Oliveira CS, Hao H, Penzien J (1991) Ground motion modeling for multiple-input structural analysis. Struct Saf 10:79–93
Pavic R, Koller MG, Bard PY, Lacave-Lachet C (2000) Ground motion prediction with the empirical Grenn's function technique: an assessment of uncertainties and confidence level. J Seismol 4:59–77
Petrovski J, Milutinovic Z (1981) Deconvolution analysis of surface accelerogram records in El-Asnam region. Actes des journées scientifiques sur le séisme d'El-Asnam du 10.10.80, Alger, 15-16 Juin:373–401
Pitarka A (1999) 3D elastic finite-difference modelling of seismic motion using staggered grids with nonuniform spacing. Bull Seismol Soc Am 89:54–68
Ramadan O, Novak M (1993) Coherency functions for spatially correlated seismic ground motions, Geotechnical Research Centre Report No. GEOT 9 93, The University of Western Ontario, London, Canada, 1993
Roumelioti Z, Kiratzi A, Thcodulidis N, Papaioannou C (2000) A comparative study of a stochastic and deterministic simulation of strong ground motion applied to the Kozani-Grevena (NW Greece) 1995 sequence. Ann Geophys 43(5):951–966
Rupakhety R, Sigbjörnsson R (2012) Spatial variability of strong ground motion: novel system-based technique applying parametric time series modelling. Bull Earthq Eng 10:1193–1204
Rupakhety R, Sigbjörnsson R (2013) Rotation-invariant measures of earthquake response spectra. Bull Earthq Eng 11:1885–1893
Rupakhety R, Sigbjörnsson R (2014a) Three-dimensional characteristics of strong-ground motion in the near-fault area. In Proceedings of the second European conference on earthquake engineering and seismology, Istanbul, 25–29 Aug 2014
Rupakhety R, Sigbjörnsson R (2014b) Rotation-invariant formulation of strong ground-motion parameters. In Proceedings of the second European conference on earthquake engineering and seismology, Istanbul, 25–29 Aug 2014

Rupakhety R, Halldorsson B, Sigbjörnsson R (2010) Estimating coseismic deformations from near source strong motion records: methods and case studies. Bull Earthq Eng 8(4):787–811

Santa-Cruz S, Heredia-Zavoni E, Harichandran RS (2000) Low-frequency behavior of coherency for strong ground motions in Mexico city and Japan. In: 12th World conference in earthquake engineering, Auckland, New-Zealand, Paper No. 76:1–8

Schneider JF, Abrahamson NA, Stepp JC (1992) The spatial variability of earthquake ground motion and effects of local site conditions. In Proceedings of the 10th world conference earthquake engineering, Madrid, Spain, vol 2, pp 967–972

Shinouzuka M, Deodatis G, Harada T (1987) Digital simulation of seismic ground motion. Technical Report NCEER-87-0017

Smerzini C, Villani M (2012) Broadband numerical simulations in complex near field geological configurations: the case study of the Mw 6.3 2009 L'Aquila earthquake. Bull Seismol Soc Am 102:2436–2451

Somerville PG, McLaren JP, Saikia CK (1988). Site-specific estimation of spatial incoherence of strong ground motion. In: Proceedings Earthquake Engineering and Soil Dynamics II, recent advances in ground-motion evaluation. ASCE, Park City, Utah, pp 188–202

Somerville PG, Mclaren JP, Sen MK, Helmberger DV (1991) The influence of site condition on the spatial incoherence of ground motions. Struct Saf 10:1–13

Spudich P (1994) Recent seismological insights into the spatial variation of earthquake ground motions. In: Proceedings of ATC-35 Seminar on New developments in earthquake ground motion estimation and implications for engineering design practice, ATC 35-1, pp 13.1–13.31

Suzuki S, Asano K (2000) Simulation of near source ground motion and its characteristics. Soil Dyn Earthq Eng 20:125–136

Walling M, Abrahamson N (2007) Spatial coherency of ground motions for embedded structures. In: 4th International conference on earthquake geotechnical engineering, Thessaloniki, Greece

Yielding G, Jackson JA, King GCP, Sinvhal H, Vita-Finzi C, Wood RM (1981) Relations between surface deformation, fault geometry, seismicity, and rupture characteristics during the E1-Asnam (Algeria) earthquake of 10 October 1980. Earth Planet Sci Lett 56:287–304

Zerva A (1994) On the spatial variation of seismic ground motions and its effects on lifelines. Eng Struct 16(7):534–546

Zerva A (2009) Spatial variation of seismic ground motions. Modeling and engineering applications. CRC Press, Boca Raton

Zerva A, Harada T (1997) Effect of surface layer stochasticity on seismic ground motion coherence and strain estimates. Soil Dynamics and Earthquake Engineering 16:445–457

Zerva A, Shinozuka M (1991) Stochastic differential ground motion. Struct Saf 10:129–143